Journal of Polymers and the Environment (2021) 29:2964–2977
https://doi.org/10.1007/s10924-021-02089-3

ORIGINAL PAPER

Isolation and Characterization of Cellulose Nanocrystals from Different Lignocellulosic Residues: A Comparative Study

Tesfaye Gabriel[1,4] · Anteneh Belete[1] · Gerd Hause[2] · Reinhard H. H. Neubert[3,4] · Tsige Gebre-Mariam[1]

Accepted: 2 February 2021 / Published online: 20 February 2021

Abstract

Recently, cellulose nanocrystals (CNCs) have captured the interest of researchers and industries. In this study, CNCs were isolated from four abundant lignocellulosic byproducts: *teff* (*Eragrostis tef*, Poaceae) straw, *enset* (*Ensete ventricosum*, Musaceae) fiber (EF), sugarcane (*Saccharum officinarum*, Poaceae) bagasse and coffee (*Coffea arabica*, Rubiaceae) hull (CH). Cellulose fibers were obtained using chlorine-free extraction with 5% sodium hydroxide pretreatment followed by delignification (with formic acid, acetic acid and hydrogen peroxide) and bleaching (with alkaline hydrogen peroxide). CNCs were then isolated following hydrolysis of the cellulose fibers with 64% sulfuric acid. The as-obtained CNCs were investigated and characterized in terms of yield, crystallinity, chemical functionality, morphology, particle size, zeta potential (ZP) and thermal stability. The CNCs displayed a typical crystal lattice of I_{β}-type based on XRD patterns, d-spacings and Z-values. The highest yield (~70%), CrI (~86%), and crystal size (~6 nm) were observed in EF–CNCs, and the least in CH–CNCs (yield: ~25%, CrI: ~77%, crystal size: ~4 nm). FTIR spectra of all CNCs indicated typical chemical composition of cellulose. TEM observations revealed that the CNCs were needle-shaped nanoscale structures with different aspect ratios (17.32–36.67) and dimensions (average length: 154.28–193.06 nm; diameter: 5.16–11.79 nm), while the DLS measurements provided the hydrodynamic sizes, 96.96–184.90 nm. The thermal studies by TGA/DTG revealed the CNCs had a two-step decomposition process at T_{max} 215–225 °C and 340–355 °C. This study showed that the CNCs isolated exhibited high crystallinity, aspect ratio, colloidal and thermal stability although differences were observed due to variations in cellulose sources.

Keywords Cellulose nanocrystals · Teff straw · Enset fiber · Sugarcane bagasse · Coffee hull

Abbreviations

C1 and C2	Cellulose fibres extracted with extraction Conditions 1 and 2, respectively
CC	Commercial cellulose
CC-CNCs	Cellulose nanocrystals isolated from commercial cellulose
CH	Coffee hull
CNCs-C1 and CNCs-C2	Cellulose nanocrystals isolated from C1 and C2, respectively
CrI(s)	Crystallinity index/indexes
DLS	Dynamic light scattering
DTG	Differential thermo gravimetry
EF	*enset* Fiber
FTIR	Fourier-Transform Infrared spectroscopy
HA	Hermans et al. approach
SA	Segal et al. approach
SB	Sugarcane bagasse
TEM	Transmission electron microscopy
TGA	Thermogravimetric analysis
TS	*teff* Straw
X_{200}	The proportion of crystallite interior chains for the 200 plane
XRD	X-ray diffraction
ZP	Zeta potential

✉ Tsige Gebre-Mariam
tsige.gmariam@aau.edu.et

[1] Department of Pharmaceutics and Social Pharmacy, School of Pharmacy, College of Health Sciences, Addis Ababa University, Addis Ababa, Ethiopia

[2] Microscopy Unit, Biocenter of the University, Martin Luther University of Halle-Wittenberg, Halle (Saale), Germany

[3] Department of Pharmaceutical Technology and Biopharmaceutics, Institute of Pharmacy, Martin Luther University Halle-Wittenberg, Halle (Saale), Germany

[4] Institute of Applied Dermatopharmacy, Martin Luther University Halle-Wittenberg, Halle (Saale), Germany

$\Delta d/d_{200}$	The fractional variation in the plane spacing for the 200 plane
τ_{200}	Average thickness (size) of cellulose crystallites for the 200 plane

Introduction

Cellulose, the most abundant polysaccharide on Earth, is the biosynthetic product from plants, animals, or bacteria. Because of its unique properties such as abundance, biodegradability, cost effectiveness, light weight, high tensile strength and stiffness, cellulose is widely used in various industries [1, 2].

Woody plants and cotton are the major sources of cellulose and cellulose derivatives for different industrial applications mainly in pharmaceutical, textile, energy and paper industries, but different factors such as economic and environmental concerns have forced researchers and stakeholders to look for other potential substitutes [3]. Additionally, it is reported that agro-industrial fibers have low cost, huge availability, and are easy to collect and are attractive alternative materials to wood, cotton, and linter [4].

Nanocelluloses are natural materials with defined nanoscale structural dimensions. The three main classes of nanocelluloses are (a) cellulose nanocrystals (CNCs), also referred to as nanocrystalline cellulose and cellulose nanowhiskers, (b) cellulose nanofibrils, also referred to as nanofibrillated cellulose, and (c) bacterial cellulose [5, 6].

CNCs are biopolymeric materials with diameter of 5–30 nm and length of 100–500 nm having needle- or rod-like crystal structure. CNCs have unique physicochemical properties such as higher surface area, reactive hydroxyl group in the surface, biocompatibility, etc. Consequently, CNCs have captured the interest of researchers and industries as they are suitable for many advanced functional applications such as tissue engineering, drug delivery, reinforcement of composite materials, template for nanomaterial synthesis, protein or enzyme immobilization, emulsion stabilizer, etc. [5, 7].

CNCs have been isolated from different lignocellulosic resources such as cotton gin motes and cotton gin waste [8], pineapple crown waste or peel [9–11], banana pseudo-stem residue [12], sago fronds [13], oil palm empty fruit bunch pulp [14], wheat bran [15], *Posidonia oceanica* waste biomass [16], seaweed (*Gelidiella aceroso*) [17], mandacaru (*Cereus jamacaru* DC.) spines [18], lemon seeds [19] and so on.

CNCs are isolated by various methods such as acid hydrolysis, ammonium persulfate and 2,2,6,6-tetramethylpiperidine 1-oxyl (TEMPO)-mediated oxidation [19], deep eutectic solvent [20], ball mill assisted solid acid hydrolysis [21], enzyme-assisted hydrolysis, mechanical disintegration and high-pressure homogenization [22]. Acid hydrolysis is the most effective method for CNCs isolation. Most authors reported the use of sulfuric acid for preparation of CNCs due to its versatile tuning of the surface charge density that endows CNCs suspensions higher colloidal stabilities [11, 12, 23], but others also reported nitric acid [24], phosphoric acid [25, 26], phosphotungstic acid [27], hydrochloric acid [28, 29], citric/hydrochloric acid hydrolysis [26] and hydrobromic acid [30].

CNCs are usually prepared from extracted cellulose fibers or highly refined cellulose products. The chemical treatment process can alter the physicochemical properties of the cellulose fibers [8]. In most studies, alkaline treatment and bleaching with sodium chlorite solutions are commonly employed for extraction of cellulose fibers prior to isolation of CNCs [8, 15, 19, 26, 31].

In this study, four abundantly available lignocellulosic byproducts namely, teff straw (TS), enset fiber (EF), sugarcane bagasse (SB) and coffee hull (CH) were used for chlorine-free extraction of cellulose fibers and CNCs.

Teff (*Eragrostis tef*, Poaceae) is one of the most commonly cultivated staple food crops for the majority of people in Ethiopia. TS is the solid byproduct generated in large quantities during threshing to obtain starch-rich tiny *teff* grains [32, 33]. *Enset* (*Ensete ventricosum*, Musaceae), a unique crop and perennial herb plant resembling banana, provides the staple food for around 20 million Ethiopians. EF is extracted mainly from the pseudostem and leaves, largely as a byproduct [34, 35]. Sugarcane (*Saccharum officinarum*, Poaceae) plays a significant role in the Ethiopian economy. The booming sugar industries in Ethiopia aiming for annual production of 3.9–4.17 million tons of sugar, and 181 million L ethanol will generate massive cellulose-rich SB [36]. Ethiopia, a leading coffee (*Coffea arabica*, Rubiaceae) producer (441,000 metric tons) in Africa, ranks the fifth largest producer and tenth exporter globally [37]. During coffee bean processing, large amounts of byproducts mainly CH, are generated and discarded or dumped into a landfill [38].

To the best of our knowledge, no work has been reported on extraction and characterization of CNCs from the abundant lignocellulosic materials: TS, EF, and CH for potential value-added applications. Isolation of CNCs from SB was included due to its massive abundance and for comparison purposes.

Materials and Methods

Materials

TS and EF were purchased from Merkato and Doyogena, local markets in Addis Ababa and Kambata Tembaro Zone,

Ethiopia, respectively. SB and CH were supplied by the Metehara Sugar Factory and the Ethiopian Coffee Processing and Warehouse Enterprise, Ethiopia, respectively. Glacial acetic acid (Riedel-de Haën), sodium hydroxide 97% (HiMedia, Mumbai, India), sulfuric acid 97% (BDH, England), formic acid (98%) (Central Drug House (P) Ltd. New Delhi, India), commercial cellulose (CC) (LOBA CHEMIE-Laboratory, India), and hydrogen peroxide 30% (CARLO ERBA reagents, France) were used as received.

Preparation of CNCs

Cellulose Extraction

Cellulose fibers were extracted from the four plant byproducts: TS, EF, SB and CH following a three-stage treatment reported in our previous work [39]. Briefly, the plant byproducts (each 20 g) were pretreated with 5% NaOH (for extraction condition 1) or 10% NaOH (for extraction condition 2), 1/10 (w/v) solid/liquid ratio of dry material on a water bath at 90 °C for 1.5 h. Pulps of the byproducts were filtered and washed continuously with hot distilled water. At delignification stage, the pulps were further treated with a mixture of 20% formic acid (FA)/20% acetic acid (AA)/7.5% H_2O_2 (2:1:2) solution on water bath at 90 °C for 1.5 h, at a byproduct to liquor ratio of 1:10 with continuous washing with hot water. Finally, the pulps were bleached with 7.5% H_2O_2 in alkaline media (adding 8 g of NaOH) at 1:10 fiber ratio, first at room temperature for 30 min, then on water bath at 70 °C for 30 min. Finally, the pulps were washed repeatedly with hot distilled water to remove residual lignin, and dried in an oven (Kottermann® 2711, Germany) for 24 h at 60 °C. The extracted celluloses following extraction condition 1 and 2 were designated as C1 and C2, respectively.

Acid Hydrolysis

First, the extracted celluloses (C1 or C2) from the plant byproducts, and CC were hydrolyzed with 64% (w/w) sulfuric acid (1:20 g/mL) at 45 °C for 30 min under vigorous stirring at 1500 rpm (the resulting NCs designated as CNCs-C1 and CNCs-C2, CC-CNCs). Immediately following the hydrolysis, the suspension was diluted tenfold with chilled distilled water to quench the hydrolysis reaction, and centrifuged successively at 4 °C (Beckman Coulter Avanti J-20 XP Centrifuge, USA) for 10 min each at 9000 rpm to remove the excess acid. The precipitate was then dialyzed in dialysis sacks (Avg. flat width 35 mm, MWCO 12,000 Da, Sigma-Aldrich, USA) with distilled water to remove non-reactive sulfate groups, salts and soluble sugars, until neutral pH was reached (5 days). Subsequently, the resulting suspension of dialysis process was treated using a disperser type UltraTurrax (Janke and Kunkel IKA-Labortechnik, Ultra-Turrax T50) for 5 min at 10,000 rpm twice and sonicated (Bandelin SONOREX Digital 10P, Sigma-aldrich) for 5 min. The aqueous suspension thus obtained was freeze-dried in a lyophilizer (Martin Christ Gefrieetrocknungsanlagen GmbH, CHRIST, An der UnterenSöse 50, 37520 Osterode am Harz, Germany) and dried for 72 h to obtain CNCs powder [2, 40–42].

Yield Determination

The yields of CNCs were estimated gravimetrically, following successive extractions of celluloses from the byproducts, and CNCs from as-extracted cellulose fibers.

Determination of Chemical Composition

The chemical compositions of the untreated plant byproducts and the as-extracted celluloses, such as cellulose, lignin, and hemicellulose contents were determined according to the methods stated elsewhere [39, 43–45], as described in the supplementary material.

X-ray Diffraction (XRD)

The crystallinity of as-isolated CNCs and cellulose precursors was analyzed with an XRD-7000 X-ray Diffractometer MAXima (SHIMADZU Corporation, Japan) at 40 kV, 30 mA with monochromatic Cu-Kα radiation, typically with scan speed of 3.0000°/min and sampling pitch of 0.0200°. Data acquired were plotted in Origin Pro 8.5.1 in a 2θ scale from 10 to 40.

The crystalline indexes (CrI) were determined following two Eqs. (1 and 2) [1, 46, 47]: (a) equation proposed by Segal et al. (Empirical method):

$$CrI = \frac{(I_{200} - I_{am})}{I_{200}} \times 100\% \quad (1)$$

where I_{200} is the maximum intensity (in arbitrary units) of the diffraction from the 200 plane, and I_{am} is the intensity of the background scatter.

(b) Hermans et al. equation (Peak deconvolution method):

$$CrI = \frac{A_{cry}}{A_{total}} \times 100\% \quad (2)$$

where A_{cry} is the sum of crystalline band areas; and A_{total} is the total area under the diffractograms.

XRD diffractograms of the as-isolated CNCs and cellulose precursors were deconvoluted following Gaussian profile, and parameters such as d-spacings (d), apparent crystallite size or thickness for the 200 plane (τ_{200}), the proportion of crystallite interior chains for the 200 plane (X_{200}), fractional variation in the plane spacing for the 200 plane

$(\Delta d/d)_{200}$, and Z-values were determined using equations described elsewhere (3–7) [1, 48, 49].

The d-spacings were calculated using the Bragg equation:

$$d = \frac{\lambda}{2sin\,\theta} \tag{3}$$

where, λ is the wavelength of the incident X-rays, d is the interplanar spacing of the crystal and θ is the angle of incidence.

The average thickness of cellulose crystallites was estimated from the XRD patterns by using Scherrer's equation:

$$\tau = \frac{\kappa\lambda}{\beta_{1/2}\cos\theta} \tag{4}$$

where τ is the crystallite dimension/size, κ is the correction factor and usually taken to be 0.94, λ is the radiation wavelength (0.1542 nm), θ is the diffraction angle corresponding to 200 plane and $\beta_{1/2}$ is the peak width at half maximum intensity.

The proportion of crystallite interior chains (X) is calculated using the equation:

$$X = \frac{(\tau - 2h)^2}{\tau^2} \tag{5}$$

where τ is the apparent crystallite size for the reflection of plane (200), and h = 0.57 nm is the layer thickness of the surface chain.

Also, the fractional variation in the plane spacing Δd/d for the 200 plane was calculated following the equation:

$$\frac{\Delta d}{d} = \frac{\beta}{2tan\,\Theta} \tag{6}$$

The Z-value indicates whether cellulose is I_α or I_β. The function that discriminates between I_α or I_β is given by equation:

$$Z = 1693d1 - 902d2 - 549 \tag{7}$$

where d_1 is the d-spacing of the (1–10) peak and d_2 is the d-spacing of the (110) peak.

Fourier-Transform Infrared (FTIR) Spectroscopy

The FTIR spectra of the as-isolated CNCs as well as cellulose precursors, and CC were examined with a Perkin Elmer FTIR spectrometer (L1600400 Spectrum TWO DTGS, SN: 108152, LIantrisant, UK) in the infrared range from 4000 to 450 cm^{-1}, with no further sample preparation.

Transmission Electron Microscopy (TEM)

A diluted CNC suspension of 0.05% (w/v) was prepared by sonication and then a drop of the suspension was deposited on a formvar-coated copper grid. The specimen was negatively stained with 1% (w/v) phosphotungstic acid solution and dried at room temperature. Images of CNCs-1 samples were taken with an EM 900 TEM (Carl Zeiss Microscopy, Jena, Germany; acceleration voltage 80 kV). Electron micrographs were taken with a slow scan camera (Variospeed SSCCD camera SM-1 k-120, TRS, Moorenweis, Germany).

Particle Size Analysis

The hydrodynamic size of the CNCs was measured using Malvern Instruments Zetasizer Nano ZS, dynamic light scattering (DLS) in backscattering mode at an angle of 173° and wavelength of 659 nm. The aqueous suspension of CNCs (0.05% w/v) were prepared from the freeze-dried samples. The results were averaged over three measurement cycles of 16 runs each at 25 °C after 120 s equilibration time.

Zeta Potential (ZP)

The ZP of aqueous suspension of CNCs (0.05% w/v) in 0.1 N PBS was measured with Malvern Instruments Zetasizer Nano ZS working on electrophoretic mobility. The measurements were carried out at a temperature of 25 °C after 120 s equilibration time at a wavelength of 659 nm.

Thermogravimetric Analysis (TGA)

Thermal stability of the as-obtained CNCs and cellulose precursors was determined with TGA/DTG (Differential Thermo Gravimetry)-60H (SHIMADZU Corporation, Japan). The samples were heated from room temperature to 700 °C at a heating rate of 10 °C/min and a nitrogen gas flow rate of 60 mL/min.

Results and Discussion

Effect of Isolation Conditions and Yield of CNCs

The chlorine-free cellulose extraction condition proved successful removal of lignin and hemicellulose after chemical treatments of the raw materials. Regarding the untreated materials, EF had the highest cellulose content (60.0%), followed by SB (39.5%), TS (36.7%) and CH (35.5%). TS contained comparable hemicellulose content as SB (~ 23%), but much higher than EF (~ 17%) and CH (~ 15%), and EF exhibited the lowest lignin (~ 13%) and CH the highest (18%). The cellulose content increased significantly in the as-extracted cellulose fibers, and the highest cellulose content (~ 95%) was observed in cellulose extracted from EF, followed by celluloses obtained from SB (~ 91%), TS (~ 90%), and CH (~ 80%). The two concentrations of sodium

hydroxide (5% and 10%) were used in the pretreatment step to investigate the effect of OH– concentration on the crystallinity of as-prepared cellulose, and then on CNCs, and the details are discussed under subsection: Crystallinity of the CNCs.

The key process parameters in the isolation of CNCs are mainly acid concentration, hydrolysis temperature and time. The optimal CNCs extraction condition reported by several researchers is hydrolysing the bleached or as-extracted cellulose with 64–65% sulfuric acid at 45 °C for 30–40 min [50–52], at fiber to acid ratio of 1:20 (g/ml), and homogenizer speed of 10,000 rpm [52]. The yield of CNCs decreases as temperature and reaction time increase. This is attributed to the additional hydrolysis of the amorphous regions of the cellulose as well as the degradation of the crystalline structures during the process [50, 53, 54]. XRD analyses revealed that the crystallinity first increases upon hydrolysis and then decreases after long duration of hydrolysis [50, 55, 56]. Thermal stability was found to decrease as the hydrolysis time increase [50]. Furthermore, other cellulose extraction conditions also influence the properties of the CNCs to be isolated [42, 57].

A turbid white mixture of materials from TS, EF and SB cellulose fibers and yellowish dark mixture from CH cellulose were formed during acid hydrolysis. White gel-like materials from TS, EF and SB celluloses are obtained after first centrifugation (Fig. S1), however, the dark brown color of CH-CNCs may indicate the presence of relatively higher lignin content in the extracted cellulose. Apparently, untreated CH has 31% lignin content and the extracted cellulose fiber (CH-cellulose) has 8%, the highest in the studied samples [39]. Similar observations on the influence of lignin content on the color of CNCs suspensions has been reported elsewhere [40]. Cellulose degradation with concomitant color-change occurs due to the formation of carbonyl groups in the cellulose chains, and also due to the formation of colored low-molecular furan-type compounds during the thermal degradation of carbohydrates [58].

The CNCs suspensions are found to be dispersed well with a milky white colloidal appearance after 10 days of storage at cold temperature as shown in Fig. 1, due to the repulsive forces of negative charge of sulfate in CNCs. The lyophilized CNCs are also showed in Fig. 1a.

The yields of the isolated CNCs from the cellulose fibers are given in Table 1. As shown in the Table, the CNCs yield depends on the source of cellulose.

Crystallinity of the CNCs

The as-isolated CNCs-C1 and CNCs-C2 like their cellulose precursors displayed a typical crystal lattice of Cellulose I, with the main diffraction signals around 2θ values of 15°, 16°, 22° and 34° with assigned crystallographic plane of 1–10, 110, 200 and 040, respectively after deconvolution using Gaussian profile as reported elsewhere [55]. The XRD patterns of CNCs-C1, and their cellulose precursors (C1) are shown in Fig. 2. The XRD patterns of CNCs-C2, and their cellulose (C2) precursors are also depicted in the supplementary material (Fig. S2).

In this study, CrIs were determined following both Segal et al. and Hermans et al. approaches [1, 46, 47]. Higher values of CrIs were recorded following Segal et al. approach when compared to Hermans et al. approach for similar plant samples. Both approaches indicate distinct variation of CrIs during hydrolysis of cellulose using sulfuric acid (Fig. 3). As the Segal et al. approach is simple and provides useful information, it is the most frequently used approach to estimate CrI in the literature [9, 49, 59].

CNCs-C1 isolated from EF exhibited the highest CrI (85.88%), a fibrous plant material (Musaceae) followed by TS and SB (84.84% and 81.64%) (Grass/Poaceae) and CH (77.20%) (Rubiaceae) using 5% NaOH in the pretreatment stage. Generally, CrIs increased in all isolated CNCs when compared to their cellulose precursors, except in CNCs isolated from TS-C2, EF-C2 and CC. Such an increment of CrI was due to the hydrolytic scission of the glycosidic bonds releasing individual crystals and removing the amorphous domains [17, 60].

There was significant increment of the CrI of the cellulose fibers when the raw materials were pretreated with 10% NaOH instead of 5% NaOH, showing removal of considerable amount of non-cellulosic materials when the raw materials were treated with 10% NaOH, without degrading cellulose. However, no significant difference in CrI was observed in the obtained CNCs employing either of the NaOH concentrations, 5% or 10%. Hence, 10% NaOH may be used in the pretreatment stage to obtain crystalline-rich cellulose; and 5% NaOH to obtain highly crystalline CNCs.

Figure 3; Table 2 show slight reduction of crystallinity in TS-CNCs-C2 and EF-CNCs-C2, compared to CrI of their cellulose precursors extracted with 10% NaOH. Such slight reduction in crystallinity may occur upon strong acid hydrolysis of highly pure and crystalline cellulose, showing that the amorphous regions have already been degraded and the acid started to partially attack the crystalline portions. Similar findings were also reported elsewhere in CNCs isolated from different sources such as MCC [55, 56], and onion skin [61]. The CrI of all CNCs-1 increased when compared with the respective cellulose precursors extracted with 5% NaOH as depicted in Fig. 3; Table 2. As CNCs isolated from cellulose (C1) exhibited higher crystallinity and comparable yield, CNCs-C1 were considered for full characterization.

The CrI of EF-CNCs-C1 (85.88%) reported in this study was higher when compared to CrIs of CNCs isolated from other sources: pseudostems of banana plants (74–75%) [12, 62], mandacaru (*Cereus jamacaru* DC.) spines (60.0–62.7%)

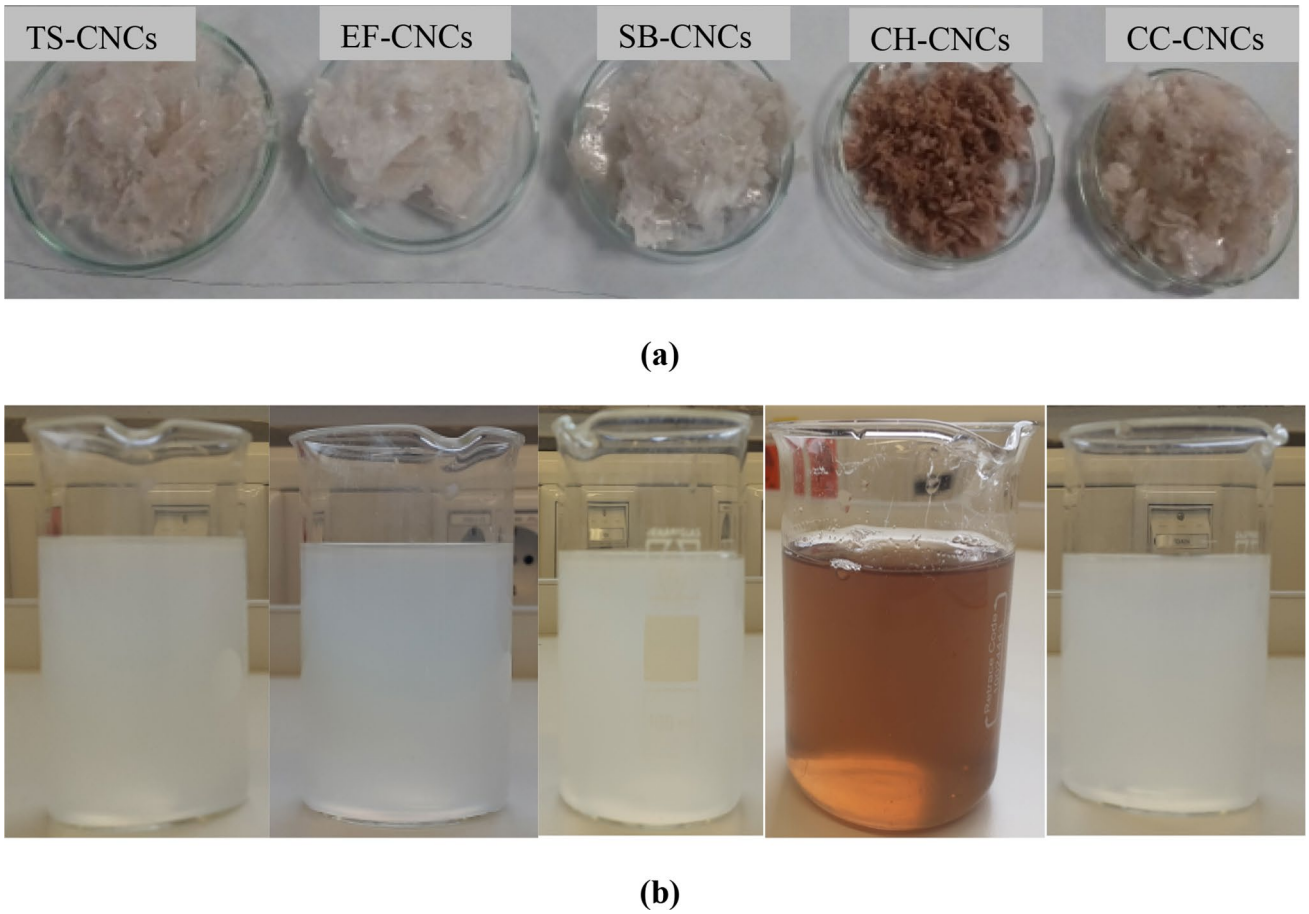

Fig. 1 Photographs of CNCs **a** lyophilized samples **b** dispersions in distilled water (0.5%) at the 10th day of storage at 4 °C (CNCs from TS, EF, SB, CH and CC from left to right). (Key: TS-*teff* straw; EF-*enset* fiber; SB-sugarcane bagasse; CH-coffee hull; *CNCs* cellulose nanocrystals; *CC* commercial cellulose included for comparison)

Table 1 Yields of celluloses and CNCs from the byproducts (Key: TS-*teff* straw; EF-*enset* fiber; SB-sugarcane bagasse; CH-coffee hull); Data are presented as the mean ± SD ($n = 3$)

Plant byproducts	Yields (%)		
	Cellulose	CNCs from cellulose	CNCs from byproducts
TS	36.7 ± 0.55	50.0 ± 3.32	18.4
EF	60.0 ± 1.25	70.0 ± 1.49	42.0
SB	39.5 ± 1.08	64.0 ± 2.79	25.3
CH	35.5 ± 1.80	25.0 ± 2.11	8.9

[18], oil palm fronds (*Elaeis guineensis*) (78.5%) [63], passion fruit (82.8%) peels waste (77.96%) [7], *Nypa Fruticans* trunk (76.6%), coconut husk fber (79.3%), and rice husk [64], pineapple crown waste (73%) [9], post-consumer wood fiberboard waste (61–71%) [31], pueraria root residue (60%) [25] and macrophyte *Typha domingensis* (74–80%) [65] following the Segal et al. approach. The CrI of SB-CNCs-C1 (81.64%) in this study is much higher than reported elsewhere 51% [66] and less than 86% [67] which may be attributed to variation in cellulose extraction conditions.

Parameters obtained from the (deconvoluted) XRD of CNCs-C1, CNCs-C2 and cellulose precursors are given in Table 2. The deconvoluted XRD patterns of the cellulose precursors and as-obtained CNCs-C1 from the lignocellulose sources are shown in Fig. S3 (supplementary material). A direct relationship was observed among CrI, crystallite sizes at the 200 plane (τ_{200} values) and the proportion of crystallite interior chains for the 200 plane (X_{200}) unlike the fractional variation in the plane spacing for the 200 plane ($\Delta d/d_{200}$) (Table 2). The X-values were used as estimates of the fraction of cellulose chains contained in the interior of the crystallites [68]. EF-CNCs-C1 exhibited the highest τ and X-values due to decreased chain mobility permitting a lower percentage of the chains to move into the perfect register of the crystals (Table 2) [48, 68] and contained the most ordered cellulose structure when compared to other CNCs. However, an inverse relationship between CrI and

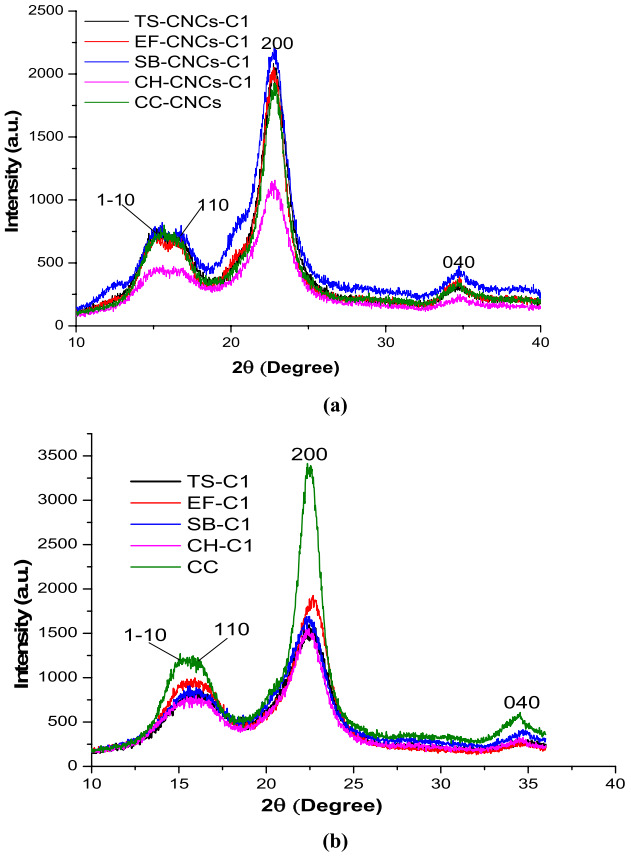

Fig. 2 XRD patterns of **a** CNCs-C1, and **b** cellulose (C1) precursors. (Key: TS-*teff* straw; EF-*enset* fiber; SB-sugarcane bagasse; CH-coffee hull; CNCs-C1-Cellulose nanocrystals isolated from cellulose (C1) extracted following Condition 1; CC-CNCs-Nanocrystals isolated from CC (commercial cellulose) included for comparison)

τ_{200} values was reported elsewhere for CNCs isolated from onion skin [61]. A greater value of the $\Delta d/d_{200}$, a measurement for the dispersion of the crystalline plane values, shows higher microstresses. EF-CNCs-C1 of this study had the lowest $\Delta d/d_{200}$ (0.0633), but the highest was recorded for TS-CNCs-C2 (0.1007). It was also reported that smaller τ_{200} value is associated with a high $\Delta d/d_{200}$ in its interplanar distance [49].

The τ values of the CNCs ranged from 4.438 nm for CH-CNCs-C1 to 5.799 nm for EF-CNCs-C1, obtained from lignocellulosic byproducts pretreated with 5% NaOH, and X values ranged from 0.552 for CH-CNCs-C1 to 0.645 for EF-CNCs-C1. The CNCs-C1 had higher τ and X values when compared to their cellulose precursors as well as CNCs-C2 except for SB-CNCs. The d-spacings of the isolated CNCs ranged from 0.541–0.600, 0.519–0.544, 0.389–0.395, and 0.257–0.260 for the planes of 1–10, 110, 200, and 040, respectively as shown in Table 2. The d-spacing values indicated that the CNCs isolated from cellulose (C1 and C2) in this study are all I_β-type cellulose [69–71] stating that the monoclinic structure is dominant in the CNCs, supported by the negative numbers of the Z-Values [72, 73].

Chemical Functionality Studies

FTIR spectra of the isolated CNCs-1, and the cellulose precursors (C1) are shown in Fig. 4. The broad band around 3333 cm^{-1} corresponds to the stretching vibrations of the OH groups in the CNCs and cellulose molecules, indicating the hydrophilic tendency of the materials. The weak transmittance band around 2890 cm^{-1} is attributed to the

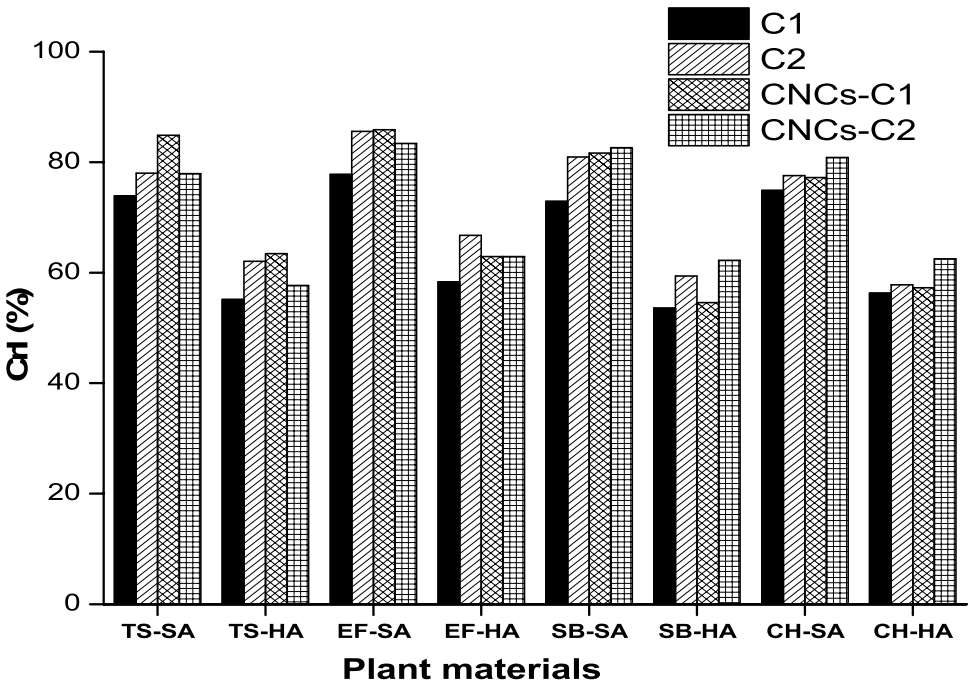

Fig. 3 Comparison of Segal et al. (SA) and Hermans et al. (HA) approaches for estimation of CrIs of the CNCs and cellulose precursors. (Key: CNCs-C1 and CNCs-C2-cellulose nanocrystals isolated from C1 and C2, respectively. TS-*teff* straw; EF-*enset* fiber; SB-sugarcane bagasse; CH-coffee hull)

Table 2 Parameters obtained from the (deconvoluted) XRD of CNCs-C1, CNCs-C2 and cellulose precursors, as well as CC-CNCs

Materials	d-spacings (nm)				τ_{200} (nm)	X_{200}	$\Delta d/d_{200}$	CrI (SA) (%)	Z-Values
	1–10	110	200	040					
TS-CNCs-C1	0.589	0.523	0.389	0.258	5.233	0.612	0.0699	84.84	– 23.69
TS-C1	0.577	0.557	0.394	0.257	2.922	0.372	0.1268	73.90	– 74.22
TS-CNCs-C2	0.593	0.544	0.395	0.259	3.682	0.477	0.1007	76.61	– 36.57
TS-C2	0.608	0.562	0.395	0.262	3.689	0.477	0.1006	78.00	– 27.64
EF-CNCs-C1	0.590	0.528	0.390	0.260	5.799	0.645	0.0633	85.88	– 26.53
EF-C1	0.580	0.559	0.392	0.270	3.973	0.509	0.0928	77.78	– 50.54
EF-CNCs-C2	0.600	0.540	0.394	0.260	5.502	0.630	0.0674	83.41	– 21.08
EF-C2	0.587	0.544	0.394	0.260	5.515	0.629	0.0668	85.56	– 45.84
SB-CNCs-C1	0.578	0.519	0.390	0.258	5.320	0.617	0.0690	81.64	– 38.84
SB-C1	0.559	0.558	0.396	0.260	3.600	0.467	0.1035	72.90	– 105.00
SB-CNCs-C2	0.589	0.528	0.394	0.260	5.366	0.620	0.0690	82.60	– 27.94
SB-C2	0.582	0.542	0.395	0.259	3.939	0.505	0.0944	80.92	– 52.41
CH-CNCs-C1	0.590	0.524	0.391	0.257	4.438	0.552	0.0827	77.20	– 21.92
CH-C1	0.606	0.560	0.397	0.259	3.618	0.469	0.1031	74.87	– 49.29
CH-CNCs-C2	0.591	0.526	0.393	0.260	5.042	0.599	0.0732	80.86	– 22.78
CH-C2	0.609	0.554	0.394	0.261	3.946	0.506	0.0938	77.59	– 16.75
CC-CNCs	0.604	0.541	0.394	0.260	4.415	0.550	0.1287	74.91	– 14.18
CC	0.608	0.554	0.395	0.260	6.480	0.679	0.0573	87.23	– 19.85

Key: C1 and C2-Cellulose extracted with Conditions A and B, respectively; CNCs-C1 and CNCs-C2-cellulose nanocrystals isolated from C1 and C2, respectively; TS-*teff* straw; EF-*enset* fiber; SB-sugarcane bagasse; CH-coffee hull; CC-Commercial cellulose included for comparison; CC-CNCs-cellulose nanocrystals isolated from commercial cellulose included for comparison; d-the interplanar spacing of the crystal; τ_{200}-average thickness of cellulose crystallites; X_{200}-the proportion of crystallite interior chains for the 200 plane; $\Delta d/d_{200}$-the fractional variation in the plane spacing for the 200 plane; CrI (SA)-crystallinity index following Segal et al. approach

asymmetric stretching vibration of the CH bond [12, 25]. The peak at ~ 1645 cm^{-1} in all the spectra corresponds to the OH bending of water absorbed into the CNCs and cellulose fiber structure [49].

A band around 1428 cm^{-1} indicates the alkane deformations relating to CH and CH_2 bending. The peak around 896 cm^{-1} is related to glycosidic C_1H deformation, a ring vibration, and OH bending where these characters infer the β-glycosidic linkages between anhydroglucose units. The transmittance peaks around 3333, 2890, 1428, 1323, 896 cm^{-1} are associated with the characteristics of native Cellulose I as seen in all cellulose and CNCs spectra, showing chemical similarity and, therefore, the acid hydrolysis did not affect the chemical structure of the cellulosic fragments [74, 75]. The FTIR spectra of CNCs-C2, and their cellulose (C2) precursors are shown in the supplementary material (Fig. S4).

Dimensional and Morphological Analyses

Appearance of needle-shaped CNCs on TEM images shows the acid hydrolysis is effective in isolating the CNCs with a scale bar of 200 nm (Fig. 5). Relatively clear images were taken for the CNCs when phosphotungstic acid solution was used rather than uranyl acetate during TEM imaging (images using uranyl acetate not shown). From the TEM analysis, the length and diameter of the CNCs isolated from the byproducts ranged from 106.78–193.06 nm and 5.16–11.79 nm, respectively. Generally, the plant CNCs range from 100–250 nm in length and 5–70 nm in diameter.

In this study, the highest aspect ratio (36.68) is observed in SB-CNCs-C1 (Table 3), which is higher than the values reported by Lam et al. (20–25) and Mueller et al. (28). Elsewhere, the CNCs obtained from SB were short and needle-shaped in the range 200–300 nm in length and 20–40 nm in diameter [76]. Reports indicate that CNCs with high aspect ratios (above 10) exhibit good mechanical properties (bending strength, tensile strength and Young's modulus) [66].

Needle-shaped particles were observed at 30 min of hydrolysis time in the current study. It was reported an increase in the acid hydrolysis time more than 60 min resulted in a significant decrease in the average length and diameter of the CNC due to the destruction of amorphous regions and even partial crystalline regions of cellulose [15].

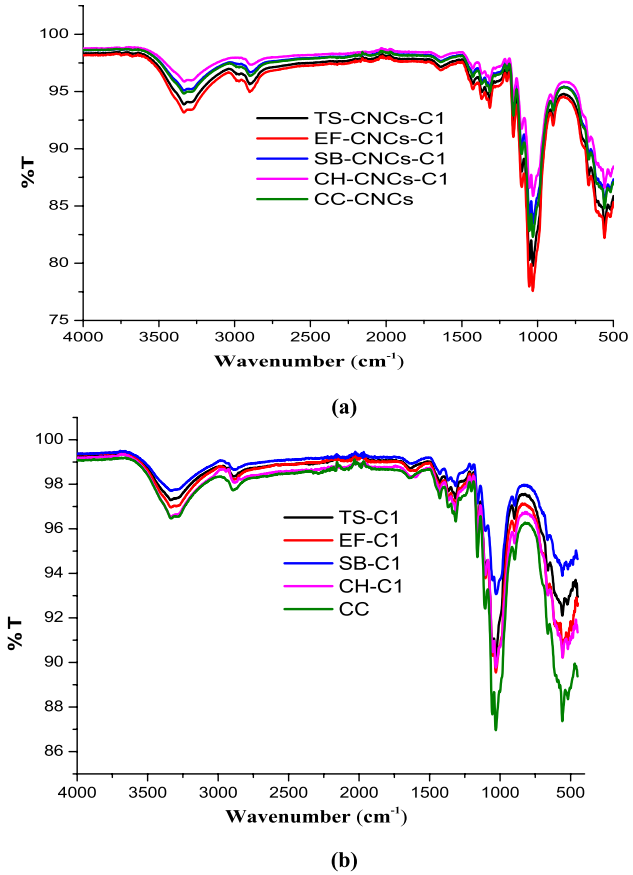

Fig. 4 FTIR spectra of **a** CNCs-C1, and **b** cellulose (C1) precursors. (Key: CNCs-C1-cellulose nanocrystals isolated from C1; C1-Cellulose extracted using extraction Condition 1; TS-*teff* straw; EF-*enset* fiber; SB-sugarcane bagasse; CH-coffee hull; CC-CNCs-cellulose nanocrystals isolated from commercial cellulose (CC) included for comparison)

Particle Size and Zeta Potential (ZP) of CNCs

The DLS results also revealed that the isolated CNCs were in nanoscale range, and their hydrodynamic size ranged from 96.96 nm of CH-CNCs-C1 to 157.2 nm of EF-CNCs-C1 with the polydispersity index (PDI) ranging from 0.209 to 0.524 (Table 4). Elsewhere, the hydrodynamic size of CNCs from SB ranged from 18.17 to 220 nm, with most particles accumulated beyond 37.84 nm [77] and from 115 to 130 nm [78]. The ZP values of the CNCs suspensions ranged from − 28.8 to − 38.6 mV in neutral water (Table 4), and resulted in stable colloidal suspensions as the absolute values obtained are higher than − 15 mV which is the minimum value to represent the onset of agglomeration [79, 80]. The negatively charged surfaces on CNCs were due to the insertion of sulfate during sulfuric acid hydrolysis [26, 63].

CNCs at the ZP values near or lower than − 20 mV at low concentrations remain stable [81]. The ZP absolute value of SB-CNCs-C1 (− 38.6 mV) was slightly higher than the ZP of CNCs isolated from SB in other studies: − 32.3 mV [66] and − 18.3 to − 20.97 mV [78]. The ZP absolute values greater than 30 are regarded as highly stable, indicating all the CNCs except TS-CNCs are colloidally very stable, and TS-CNCs with ZP value of − 28.8 mV are considered to be moderately stable (Table 4) [26]. It was reported elsewhere that the ZP absolute value increased significantly from − 8.7 to − 95.3 mV when the acid hydrolysis time increased from 20 to 120 min [50].

Thermal Properties of the CNCs

The thermal properties of the CNCs-1, and cellulose precursors (C1) from each byproduct were investigated with TGA/Differential thermogravimetry (DTG). The isolated CNCs presents three main weight loss regions, as shown in Fig. 6a, b, and the supplementary material (Fig. S5 and Table S1). The initial small (3.8–5.7%) weight loss in the region 30–110 °C (with maximum weight loss temperature from 60 to 64 °C) is mainly due to moisture evaporation; water adsorbed to the isolated CNCs [15, 25, 82, 83].

All CNCs displayed a two-step decomposition process, along with the appearance of small shoulders around 160 °C in DTG (evident in TS-CNCS, EF-CNCs and CC-CNCs). A weight loss of 29–38% was observed in the first step decomposition temperature of the CNCs (T_{max} 215–225 °C) and this is due to the degradation of both surface sulfate groups and CNCs. Other studies have shown the lower thermal stability of CNCs is due to its large specific surface area and the sulfated group of the CNCs [15, 82, 84].

The second decomposition step exhibited at T_{max} ranging from ~ 340 to 355 °C (the major cellulose degradation temperature), due to breakdown of the interior non-sulfated cellulose crystals and a few studies in the literature also reported similar behavior for CNCs isolated from plant materials such as SB [84], Tetra pak Cellulose I [82], corncob [83] and pineapple crown waste [9]. The weight loss ranged from 18.5 to 25.4%, which is slightly lower than the former phase of decomposition. All the isolated CNCs exhibited lower maximum weight loss rates (0.1760 to 0.2050%/°C) in the sulfated cellulose groups than cellulose precursors. The charred residues at 550 °C of all CNCs showed higher values than cellulose counterparts because of a dehydration effect of the sulfate group as flame retardants [61, 82, 83].

The thermal degradation properties of as-extracted cellulose fibers are depicted in Fig. 6c, d, and Table S1. A maximum weight loss of the cellulose fibers (50–70%) was observed at the maximum degradation temperatures ranging from 330 to 360 °C. This might be due to several degradation factors such as depolymerization, dehydration and decomposition of the glycosidic units of the cellulose chains as reported elsewhere [85]. The higher thermal stability of the as-extracted cellulose fibers

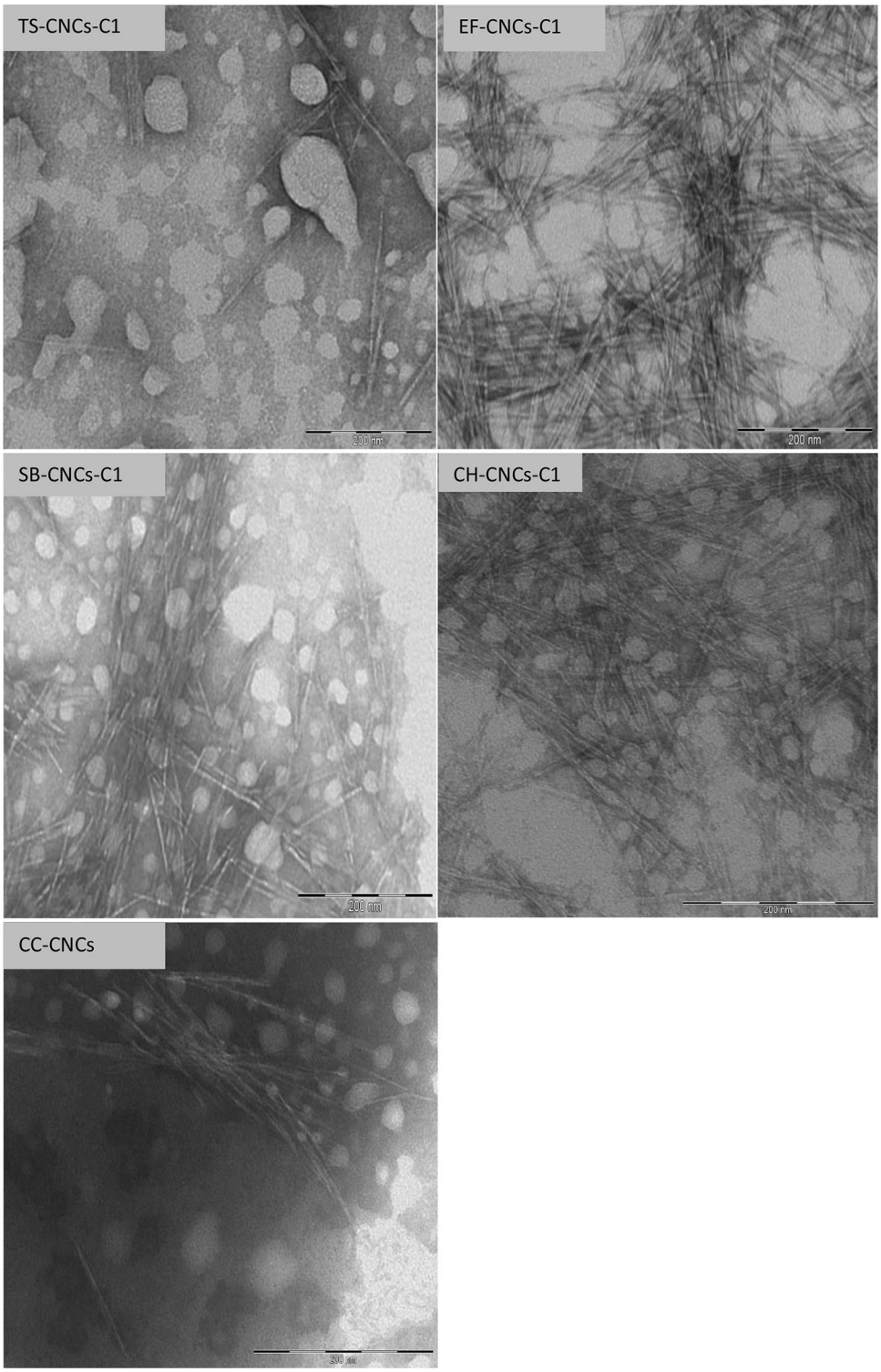

Fig. 5 Transmission electron micrographs of CNCs-1 (TS-CNCs-C1, EF-CNCs-C1, SB-CNCs-C1, CH-CNCs-C1), and CC-CNCs) (Bar scale: 200 nm). (Key: CNCs-C1-cellulose nanocrystals isolated from C1; C1-Cellulose extracted using extraction Condition 1; TS-*teff* straw; EF-*enset* fiber; SB-sugarcane bagasse; CH-coffee hull; CC-CNCs-cellulose nanocrystals isolated from commercial cellulose (CC) included for comparison)

from the raw materials is related to their high crystallinity. The maximum weight loss rate of the cellulose fibers ranged from 0.5795%/°C for CH-C1 (at 329.73 °C) to 1.6756%/°C for EF-C1 (at 340.30 °C). The TGA/DTG curves of as-extracted cellulose fibers showed the removal of hemicelluloses and lignin by the chlorine-free extraction conditions confirming successful cellulose extraction process [86].

Table 3 TEM dimensional analysis of CNCs isolated from cellulose (C1) extracted from various raw materials

Source (CNCs)	Length (L) range; $L_{average}$ (nm)	Diameter (D) range; $D_{average}$ (nm)	Aspect ratio
TS-CNCs-C1	76.96–300.08; 193.06 ± 52.41	2.25–10.88; 6.7 ± 2.08	28.82
EF-CNCs-C1	88.67–242.35; 154.28 ± 36.712	3.22–16.14; 8.889 ± 3.043	17.32
SB-CNCs-C1	110.68–301.66; 189.29 ± 49.928	2.20–8.97; 5.16 ± 1.91	36.68
CH-CNCs-C1	116.51–232.41; 188.07 ± 25.86	3.65–13.97; 7.268 ± 3.25	25.88
CC-CNCs	50.871–147.211; 106.78 ± 21.211	4.17–11.31; 6.141 ± 1.567	17.39

(Key: CNCs-C1-cellulose nanocrystals isolated from C1; C1-Cellulose extracted using extraction Condition 1; TS-*teff* straw; EF-*enset* fiber; SB-sugarcane bagasse; CH-coffee hull; CC-CNCs-cellulose nanocrystals isolated from commercial cellulose (CC) included for comparison, $L_{average}$-average length; $D_{average}$-average diameter of CNCs estimated using ImageJ Software)

Table 4 Hydrodynamic size using DLS and Zeta Potential (ZP) values

SN	Source (CNCs)	Hydrodynamic size (nm); PDI (DLS)	ZP (mV)
1.	TS-CNCs-C1	137.0; 0.209	− 28.8
2.	EF-CNCs-C1	157.2; 0.524	− 29.9
3.	SB-CNCs-C1	106.8; 0.285	− 38.6
4.	CH-CNCs-C1	96.96; 0.261	− 33.5
5.	CC-CNCs	184.9; 0.426	− 37.8

(Key: CNCs-C1-cellulose nanocrystals isolated from C1; C1-Cellulose extracted using extraction Condition 1; TS-*teff* straw; EF-*enset* fiber; SB-sugarcane bagasse; CH-coffee hull; CC-commercial cellulose; CC-CNCs-cellulose nanocrystals isolated from commercial cellulose included for comparison)

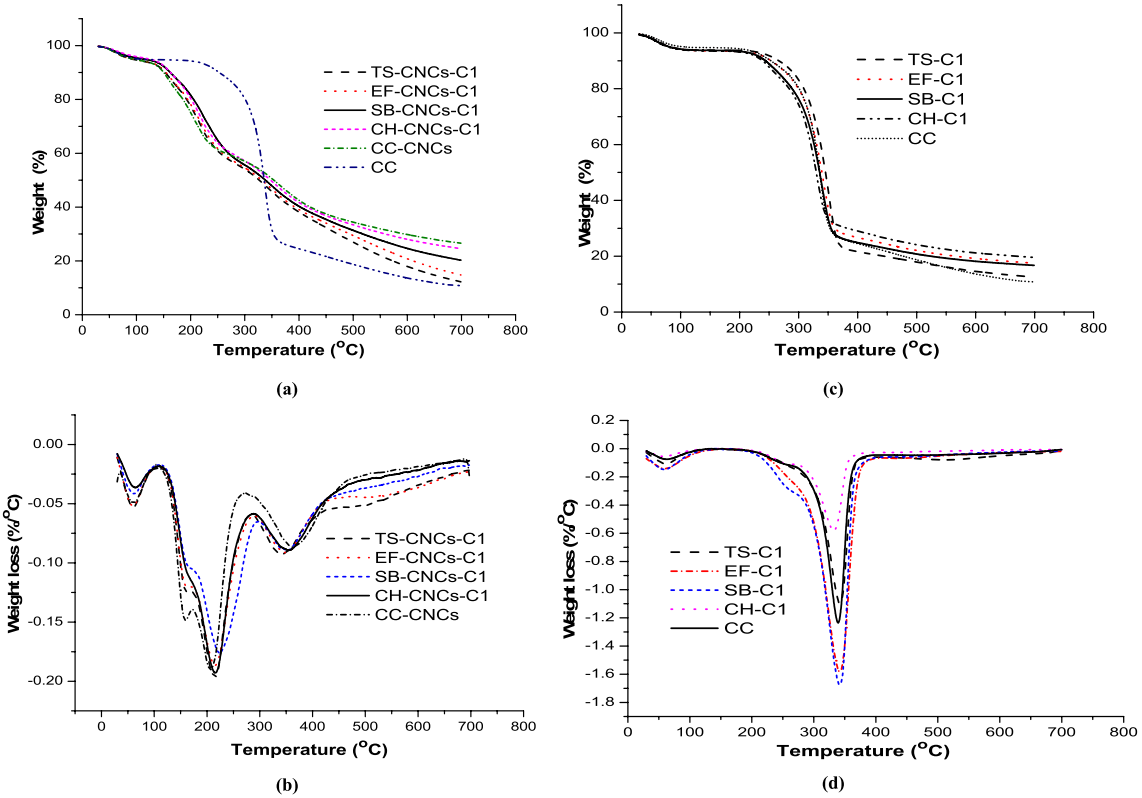

Fig. 6 Thermal degradation behaviors: **a** TGA and **b** DTG of CNCs (upper two), and **c** TGA and **d** DTG of cellulose (C1) precursors (lower two) extracted with Condition 1, and CC. (Key: CNCs-C1-cellulose nanocrystals isolated from C1; C1-Cellulose extracted using extraction Condition 1; TS-*teff* straw; EF-*enset* fiber; SB-sugarcane bagasse; CH-coffee hull; CC-CNCs-cellulose nanocrystals isolated from commercial cellulose (CC) included for comparison)

Conclusion

Highly crystalline CNCs were obtained from the four abundant byproducts: TS, EF, SB and CH with chlorine-free cellulose extraction and sulfuric acid hydrolysis. The highest yield, CrI and crystal size were exhibited in EF-CNCs, and the least in CH-CNCs. No polymorphic transition occurred during cellulose extraction and acid hydrolysis. A direct relationship was observed among CrIs, crystallite sizes (τ_{200}) and the proportion of crystallite interior chains (X_{200}) in the as-obtained CNCs. A two-step decomposition process of CNCs was observed and this was due to degradation of surface sulfate groups and large specific surface area, and breakdown of the interior non-sulfated cellulose crystals. Based on the findings (high yield, CrI and aspect ratio), the four lignocellulosic materials can be used as alternative sources of CNCs.

Supplementary Information The online version contains supplementary material available at https://doi.org/10.1007/s10924-021-02089-3.

Acknowledgements The authors would like to acknowledge Addis Ababa University, Ethiopia for sponsoring the PhD study of TG, and Martin Luther University, Germany for providing access to laboratory space and facilities such as TEM and DLS. This research was partly supported by the Ministry of Innovation and Technology, Ethiopia, and Tri-Sustain (Economic, Ecological and Therapeutic Sustainability) Project in the development of phytopharmaceuticals for Sub-Saharan Africa, funded by the German Ministry of Research and Education (BmBF) (Grant No. 01DG17008B) and German Academic Exchange Service (DAAD) (Grant No. 57369155), Germany.

Author Contributions Conceptualization, Methodology, Investigation, Visualization, original draft Writing, Software: TG. Writing—review & editing, Formal analysis: AB. Software, Methodology, Writing—review & editing: GH. Funding acquisition, Project administration, Writing—review & editing: RN. Conceptualization, Investigation, Supervision, Visualization, Writing—review & editing, Funding acquisition: TG-M.

References

1. Poletto M, Ornaghi Júnior HL, Zattera AJ (2014) Native cellulose: Structure, characterization and thermal properties. Materials (Basel) 7:6105–6119. https://doi.org/10.3390/ma7096105
2. El Achaby M, El Miri N, Hannache H et al (2018) Production of cellulose nanocrystals from vine shoots and their use for the development of nanocomposite materials. Int J Biol Macromol 117:592–600. https://doi.org/10.1016/j.ijbiomac.2018.05.201
3. Adel AM, Abd El-Wahab ZH, Ibrahim AA, Al-Shemy MT (2011) Characterization of microcrystalline cellulose prepared from lignocellulosic materials. Part II: physicochemical properties. Carbohydr Polym 83:676–687. https://doi.org/10.1016/j.carbpol.2010.08.039
4. do Nascimento DM, Dias AF, de Araújo Junior CP et al (2016) A comprehensive approach for obtaining cellulose nanocrystal from coconut fiber. Part II: environmental assessment of technological pathways. Ind Crops Prod 93:58–65. https://doi.org/10.1016/j.indcrop.2016.02.063
5. Abitbol T, Rivkin A, Cao Y et al (2016) Nanocellulose, a tiny fiber with huge applications. Curr Opin Biotechnol 39:76–88. https://doi.org/10.1016/j.copbio.2016.01.002
6. Klemm D, Cranston ED, Fischer D et al (2018) Nanocellulose as a natural source for groundbreaking applications in materials science: today's state. Mater Today 21:720–748. https://doi.org/10.1016/j.mattod.2018.02.001
7. Wijaya CJ, Saputra SN, Soetaredjo FE et al (2017) Cellulose nanocrystals from passion fruit peels waste as antibiotic drug carrier. Carbohydr Polym 175:370–376. https://doi.org/10.1016/j.carbpol.2017.08.004
8. Jordan JH, Easson MW, Dien B et al (2019) Extraction and characterization of nanocellulose crystals from cotton gin motes and cotton gin waste. Cellulose 26:5959–5979. https://doi.org/10.1007/s10570-019-02533-7
9. Prado KS, Spinacé MAS (2019) Isolation and characterization of cellulose nanocrystals from pineapple crown waste and their potential uses. Int J Biol Macromol 122:410–416. https://doi.org/10.1016/j.ijbiomac.2018.10.187
10. Pereira PHF, Ornaghi Júnior HL, Coutinho LV et al (2020) Obtaining cellulose nanocrystals from pineapple crown fibers by free-chlorite hydrolysis with sulfuric acid: physical, chemical and structural characterization. Cellulose 27:5745–5756. https://doi.org/10.1007/s10570-020-03179-6
11. Dai H, Ou S, Huang Y, Huang H (2018) Utilization of pineapple peel for production of nanocellulose and film application. Cellulose 25:1743–1756. https://doi.org/10.1007/s10570-018-1671-0
12. Meng F, Wang G, Du X et al (2019) Extraction and characterization of cellulose nanofibers and nanocrystals from liquefied banana pseudo-stem residue. Compos Part B Eng 160:341–347. https://doi.org/10.1016/j.compositesb.2018.08.048
13. Arnata IW, Suprihatin S, Fahma F et al (2020) Cationic modification of nanocrystalline cellulose from sago fronds. Cellulose 27:3121–3141. https://doi.org/10.1007/s10570-019-02955-3
14. Al-Dulaimi AA, Wanrosli WD (2017) Isolation and characterization of nanocrystalline cellulose from totally chlorine free oil palm empty fruit bunch pulp. J Polym Environ 25:192–202. https://doi.org/10.1007/s10924-016-0798-z
15. Xiao Y, Liu Y, Wang X et al (2019) Cellulose nanocrystals prepared from wheat bran: characterization and cytotoxicity assessment. Int J Biol Macromol 140:225–233. https://doi.org/10.1016/j.ijbiomac.2019.08.160
16. Benito-González I, López-Rubio A, Gavara R, Martínez-Sanz M (2019) Cellulose nanocrystal-based films produced by more sustainable extraction protocols from *Posidonia oceanica* waste biomass. Cellulose 26:8007–8024. https://doi.org/10.1007/s10570-019-02641-4
17. Singh S, Gaikwad KK, Il PS, Lee YS (2017) Microwave-assisted step reduced extraction of seaweed (*Gelidiella aceroso*) cellulose nanocrystals. Int J Biol Macromol 99:506–510. https://doi.org/10.1016/j.ijbiomac.2017.03.004
18. Nepomuceno NC, Santos ASF, Oliveira JE et al (2017) Extraction and characterization of cellulose nanowhiskers from Mandacaru (*Cereus jamacaru* DC.) spines. Cellulose 24:119–129. https://doi.org/10.1007/s10570-016-1109-5
19. Zhang H, Chen Y, Wang S et al (2020) Extraction and comparison of cellulose nanocrystals from lemon (*Citrus limon*) seeds using sulfuric acid hydrolysis and oxidation methods. Carbohydr Polym 238:116180. https://doi.org/10.1016/j.carbpol.2020.116180
20. Fan Q, Jiang C, Wang W et al (2020) Eco-friendly extraction of cellulose nanocrystals from grape pomace and construction of self-healing nanocomposite hydrogels. Cellulose 27:2541–2553. https://doi.org/10.1007/s10570-020-02977-2

21. Song K, Ji Y, Wang L et al (2018) A green and environmental benign method to extract cellulose nanocrystal by ball mill assisted solid acid hydrolysis. J Clean Prod 196:1169–1175. https://doi.org/10.1016/j.jclepro.2018.06.128
22. Park NM, Choi S, Oh JE, Hwang DY (2019) Facile extraction of cellulose nanocrystals. Carbohydr Polym 223:115114. https://doi.org/10.1016/j.carbpol.2019.115114
23. Dai H, Wu J, Zhang H et al (2020) Recent advances on cellulose nanocrystals for Pickering emulsions: Development and challenge. Trends Food Sci Technol 102:16–29. https://doi.org/10.1016/j.tifs.2020.05.016
24. Orasugh JT, Sarkar G, Saha NR et al (2019) Effect of cellulose nanocrystals on the performance of drug loaded in situ gelling thermo-responsive ophthalmic formulations. Int J Biol Macromol 124:235–245. https://doi.org/10.1016/j.ijbiomac.2018.11.217
25. Wang Z, Yao Z, Zhou J et al (2019) Isolation and characterization of cellulose nanocrystals from pueraria root residue. Int J Biol Macromol 129:1081–1089. https://doi.org/10.1016/j.ijbiomac.2018.07.055
26. Kassab Z, Kassem I, Hannache H et al (2020) Tomato plant residue as new renewable source for cellulose production: extraction of cellulose nanocrystals with different surface functionalities. Cellulose 27:4287–4303. https://doi.org/10.1007/s10570-020-03097-7
27. Liu Y, Wang H, Yu G et al (2014) A novel approach for the preparation of nanocrystalline cellulose by using phosphotungstic acid. Carbohydr Polym 110:415–422. https://doi.org/10.1016/j.carbpol.2014.04.040
28. Yu H, Qin Z, Liang B et al (2013) Facile extraction of thermally stable cellulose nanocrystals with a high yield of 93% through hydrochloric acid hydrolysis under hydrothermal conditions. J Mater Chem A 1:3938–3944. https://doi.org/10.1039/c3ta01150j
29. Hastuti N, Kanomata K, Kitaoka T (2018) Hydrochloric acid hydrolysis of pulps from oil palm empty fruit bunches to produce cellulose nanocrystals. J Polym Environ 26:3698–3709. https://doi.org/10.1007/s10924-018-1248-x
30. Sadeghifar H, Filpponen I, Clarke SP et al (2011) Production of cellulose nanocrystals using hydrobromic acid and click reactions on their surface. J Mater Sci 46:7344–7355. https://doi.org/10.1007/s10853-011-5696-0
31. Couret L, Irle M, Belloncle C, Cathala B (2017) Extraction and characterization of cellulose nanocrystals from post-consumer wood fiberboard waste. Cellulose 24:2125–2137. https://doi.org/10.1007/s10570-017-1252-7
32. Esayas E, Agon EC, Assefa S (2018) Development of wall construction material stabilized with Enset vegetable fibers for rural housing units. Am J Civ Eng Archit 6:54–62. https://doi.org/10.12691/ajcea-6-2-2
33. Minten B, Tamru S, Engida E, Kuma T (2016) Feeding Africa's cities: the case of the supply chain of Teff to Addis Ababa. Econ Dev Cult Change 64:265–297. https://doi.org/10.1086/683843
34. Borrell JS, Biswas MK, Goodwin M et al (2019) Enset in Ethiopia: a poorly characterized but resilient starch staple. Ann Bot 123:747–766. https://doi.org/10.1093/aob/mcy214
35. Gebre-Mariam T, Schmidt PC (1996) Isolation and physico-chemical properties of enset starch. Starch/Staerke 48:208–214. https://doi.org/10.1002/star.19960480603
36. Tena Gashaw E, Mekbib F, Ayana A (2018) Sugarcane landraces of Ethiopia: Germplasm collection and analysis of regional diversity and distribution. Adv Agric 2018:1–18. https://doi.org/10.1155/2018/7920724
37. Bickford R (2019) Ethiopia coffee annual coffee annual report—global agricultural information network
38. Wang Z, Dadi Bekele L, Qiu Y et al (2019) Preparation and characterization of coffee hull fiber for reinforcing application in thermoplastic composites. Bioengineered 10:397–408. https://doi.org/10.1080/21655979.2019.1661694
39. Gabriel T, Belete A, Syrowatka F et al (2020) Extraction and characterization of celluloses from various plant byproducts. Int J Biol Macromol 158:1248–1258. https://doi.org/10.1016/j.ijbiomac.2020.04.264
40. de Oliveira JP, Bruni GP, el Halal SLM et al (2019) Cellulose nanocrystals from rice and oat husks and their application in aerogels for food packaging. Int J Biol Macromol 124:175–184. https://doi.org/10.1016/j.ijbiomac.2018.11.205
41. Coelho CCS, Michelin M, Cerqueira MA et al (2018) Cellulose nanocrystals from grape pomace: production, properties and cytotoxicity assessment. Carbohydr Polym 192:327–336. https://doi.org/10.1016/j.carbpol.2018.03.023
42. Fortunati E, Puglia D, Monti M et al (2013) Extraction of cellulose nanocrystals from *Phormium tenax* fibres. J Polym Environ 21:319–328. https://doi.org/10.1007/s10924-012-0543-1
43. Yeasmin MS, Mondal MIH (2015) Synthesis of highly substituted carboxymethyl cellulose depending on cellulose particle size. Int J Biol Macromol 80:725–731. https://doi.org/10.1016/j.ijbiomac.2015.07.040
44. Lin L, Yan R, Liu Y, Jiang W (2010) In-depth investigation of enzymatic hydrolysis of biomass wastes based on three major components: cellulose, hemicellulose and lignin. Bioresour Technol 101:8217–8223. https://doi.org/10.1016/j.biortech.2010.05.084
45. Abdel-Halim ES (2014) Chemical modification of cellulose extracted from sugarcane bagasse: preparation of hydroxyethyl cellulose. Arab J Chem 7:362–371. https://doi.org/10.1016/j.arabjc.2013.05.006
46. Segal L, Creely JJ, Martin AE, Conrad CM (1959) An empirical method for estimating the degree of crystallinity of native cellulose using the X-ray diffractometer. Text Res J 29:786–794. https://doi.org/10.1177/004051755902901003
47. Hermans H, Hermans JJ, Vermaas D, Weidinger A (1948) Deformation mechanism of cellulose gels. IV.* General relationship between orientation of the crystalline and that of the amorphous portion. J Polym Sci 3:1–9
48. Popescu M, Popescu C, Lisa G, Sakata Y (2011) Evaluation of morphological and chemical aspects of different wood species by spectroscopy and thermal methods. J Mol Struct 988:65–72. https://doi.org/10.1016/j.molstruc.2010.12.004
49. Aguayo MG, Pérez AF, Reyes G et al (2018) Isolation and characterization of cellulose nanocrystals from rejected fibers originated in the Kraft Pulping process. Polymers (Basel) 10:1145–1156. https://doi.org/10.3390/polym10101145
50. Kargarzadeh H, Ahmad I, Abdullah I et al (2012) Effects of hydrolysis conditions on the morphology, crystallinity, and thermal stability of cellulose nanocrystals extracted from kenaf bast fibers. Cellulose 19:855–866. https://doi.org/10.1007/s10570-012-9684-6
51. Gong J, Mo L, Li J (2018) A comparative study on the preparation and characterization of cellulose nanocrystals with various polymorphs. Carbohydr Polym 195:18–28. https://doi.org/10.1016/j.carbpol.2018.04.039
52. Hemmati F, Jafari SM, Kashaninejad M, Barani Motlagh M (2018) Synthesis and characterization of cellulose nanocrystals derived from walnut shell agricultural residues. Int J Biol Macromol 120:1216–1224. https://doi.org/10.1016/j.ijbiomac.2018.09.012
53. Shaheen TI, Emam HE (2018) Sono-chemical synthesis of cellulose nanocrystals from wood sawdust using acid hydrolysis. Int J Biol Macromol 107:1599–1606. https://doi.org/10.1016/j.ijbiomac.2017.10.028
54. Hafemann E, Battisti R, Marangoni C, Machado RAF (2019) Valorization of royal palm tree agroindustrial waste by isolating

cellulose nanocrystals. Carbohydr Polym 218:188–198. https://doi.org/10.1016/j.carbpol.2019.04.086
55. Haafiz MKM, Hassan A, Zakaria Z, Inuwa IM (2014) Isolation and characterization of cellulose nanowhiskers from oil palm biomass microcrystalline cellulose. Carbohydr Polym 103:119–125. https://doi.org/10.1016/j.carbpol.2013.11.055
56. Korolovych VF, Cherpak V, Nepal D et al (2018) Cellulose nanocrystals with different morphologies and chiral properties. Polymer (Guildf) 145:334–347. https://doi.org/10.1016/j.polymer.2018.04.064
57. Di Giorgio L, Salgado PR, Dufresne A, Mauri AN (2020) Nanocelluloses from phormium (*Phormium tenax*) fibers. Cellulose 27:4975–4990. https://doi.org/10.1007/s10570-020-03120-x
58. Heggset EB, Chinga-Carrasco G, Syverud K (2017) Temperature stability of nanocellulose dispersions. Carbohydr Polym 157:114–121. https://doi.org/10.1016/j.carbpol.2016.09.077
59. Naduparambath S, Purushothaman E (2016) Sago seed shell: determination of the composition and isolation of microcrystalline cellulose (MCC). Cellulose 23:1803–1812. https://doi.org/10.1007/s10570-016-0904-3
60. García-García D, Balart R, Lopez-Martinez J et al (2018) Optimizing the yield and physico-chemical properties of pine cone cellulose nanocrystals by different hydrolysis time. Cellulose 25:2925–2938. https://doi.org/10.1007/s10570-018-1760-0
61. Rhim JW, Reddy JP, Luo X (2015) Isolation of cellulose nanocrystals from onion skin and their utilization for the preparation of agar-based bio-nanocomposites films. Cellulose 22:407–420. https://doi.org/10.1007/s10570-014-0517-7
62. Mueller S, Weder C, Foster EJ (2014) Isolation of cellulose nanocrystals from pseudostems of banana plants. RSC Adv 4:907–915. https://doi.org/10.1039/c3ra46390g
63. Dungani R, Owolabi AF, Saurabh CK et al (2017) Preparation and fundamental characterization of cellulose nanocrystal from oil palm fronds biomass. J Polym Environ 25:692–700. https://doi.org/10.1007/s10924-016-0854-8
64. Nang An V, Chi Nhan HT, Tap TD et al (2020) Extraction of high crystalline nanocellulose from biorenewable sources of Vietnamese agricultural wastes. J Polym Environ 28:1465–1474. https://doi.org/10.1007/s10924-020-01695-x
65. César NR, Pereira-da-Silva MA, Botaro VR, de Menezes AJ (2015) Cellulose nanocrystals from natural fiber of the macrophyte *Typha domingensis*: extraction and characterization. Cellulose 22:449–460. https://doi.org/10.1007/s10570-014-0533-7
66. Ferreira FV, Mariano M, Rabelo SC et al (2018) Isolation and surface modification of cellulose nanocrystals from sugarcane bagasse waste: from a micro- to a nano-scale view. Appl Surf Sci 436:1113–1122. https://doi.org/10.1016/j.apsusc.2017.12.137
67. De OFB, Bras J, Pimenta MTB et al (2016) Production of cellulose nanocrystals from sugarcane bagasse fibers and pith. Ind Crops Prod 93:48–57. https://doi.org/10.1016/j.indcrop.2016.04.064
68. Newman RH (1999) Estimation of the lateral dimensions of cellulose crystallites using 13C NMR signal strengths. Solid State Nucl Magn Reson 15:21–29. https://doi.org/10.1016/S0926-2040(99)00043-0
69. Wada M, Okano T (2001) Localization of Iα and Iβ phases in algal cellulose revealed by acid treatments. Cellulose 8:183–188. https://doi.org/10.1023/A:1013196220602
70. Kim UJ, Eom SH, Wada M (2010) Thermal decomposition of native cellulose: Influence on crystallite size. Polym Degrad Stab 95:778–781. https://doi.org/10.1016/j.polymdegradstab.2010.02.009
71. French AD (2014) Idealized powder diffraction patterns for cellulose polymorphs. Cellulose 21:885–896. https://doi.org/10.1007/s10570-013-0030-4
72. Poletto M, Zattera AJ, Forte MMC, Santana RMC (2012) Thermal decomposition of wood: influence of wood components and cellulose crystallite size. Bioresour Technol 109:148–153. https://doi.org/10.1016/j.biortech.2011.11.122
73. He Q, Wang Q, Zhou H et al (2018) Highly crystalline cellulose from brown seaweed *Saccharina japonica*: isolation, characterization and microcrystallization. Cellulose 25:5523–5533. https://doi.org/10.1007/s10570-018-1966-1
74. Yang H, Yan R, Chen H et al (2007) Characteristics of hemicellulose, cellulose and lignin pyrolysis. Fuel 86:1781–1788. https://doi.org/10.1016/j.fuel.2006.12.013
75. Mohamad Haafiz MK, Eichhorn SJ, Hassan A, Jawaid M (2013) Isolation and characterization of microcrystalline cellulose from oil palm biomass residue. Carbohydr Polym 93:628–634. https://doi.org/10.1016/j.carbpol.2013.01.035
76. Sukyai P, Anongjanya P, Bunyahwuthakul N et al (2018) Effect of cellulose nanocrystals from sugarcane bagasse on whey protein isolate-based films. Food Res Int 107:528–535. https://doi.org/10.1016/j.foodres.2018.02.052
77. Mandal A, Chakrabarty D (2011) Isolation of nanocellulose from waste sugarcane bagasse (SCB) and its characterization. Carbohydr Polym 86:1291–1299. https://doi.org/10.1016/j.carbpol.2011.06.030
78. Saha S, Ghosh R (2019) Cellulose nanocrystals from lignocellulosic agro-waste: a comparative study on conventional and ultrasonic assisted preparation methods. Mater Today Proc 11:628–636. https://doi.org/10.1016/j.matpr.2019.03.020
79. Thomas D, Latha MS, Thomas KK (2018) Synthesis and in vitro evaluation of alginate-cellulose nanocrystal hybrid nanoparticles for the controlled oral delivery of rifampicin. J Drug Deliv Sci Technol 46:392–399. https://doi.org/10.1016/j.jddst.2018.06.004
80. de Benini KCCC, Voorwald HJC, Cioffi MOH et al (2018) Preparation of nanocellulose from *Imperata brasiliensis* grass using Taguchi method. Carbohydr Polym 192:337–346. https://doi.org/10.1016/j.carbpol.2018.03.055
81. Stinson-Bagby KL, Roberts R, Foster EJ (2018) Effective cellulose nanocrystal imaging using transmission electron microscopy. Carbohydr Polym 186:429–438. https://doi.org/10.1016/j.carbpol.2018.01.054
82. Xing L, Gu J, Zhang W et al (2018) Cellulose I and II nanocrystals produced by sulfuric acid hydrolysis of Tetra pak cellulose I. Carbohydr Polym 192:184–192. https://doi.org/10.1016/j.carbpol.2018.03.042
83. Silvério HA, Flauzino Neto WP, Dantas NO, Pasquini D (2013) Extraction and characterization of cellulose nanocrystals from corncob for application as reinforcing agent in nanocomposites. Ind Crops Prod 44:427–436. https://doi.org/10.1016/j.indcrop.2012.10.014
84. Lam NT, Chollakup R, Smitthipong W et al (2017) Characterization of cellulose nanocrystals extracted from sugarcane bagasse for potential biomedical materials. Sugar Tech 19:539–552. https://doi.org/10.1007/s12355-016-0507-1
85. Bano S, Negi YS (2017) Studies on cellulose nanocrystals isolated from groundnut shells. Carbohydr Polym 157:1041–1049. https://doi.org/10.1016/j.carbpol.2016.10.069
86. Wijaya CJ, Ismadji S, Aparamarta HW, Gunawan S (2019) Optimization of cellulose nanocrystals from bamboo shoots using Response Surface Methodology. Heliyon 5:e02807. https://doi.org/10.1016/j.heliyon.2019.e02807